Remote Sensing of Environment 176 (2016) 152–162

Contents lists available at ScienceDirect

Remote Sensing of Environment

journal homepage: www.elsevier.com/locate/rse

Improved modeling of land surface phenology using MODIS land surface reflectance and temperature at evergreen needleleaf forests of central North America

Yuxia Liu [a,b], Chaoyang Wu [a,*], Dailiang Peng [c,*], Shiguang Xu [a], Alemu Gonsamo [d], Rachhpal S. Jassal [e], M. Altaf Arain [f], Linlin Lu [c], Bin Fang [g], Jing M. Chen [d]

[a] State Key Laboratory of Remote Sensing Science, Institute of Remote Sensing and Digital Earth, Chinese Academy of Sciences, Beijing 100101, China
[b] University of the Chinese Academy of Sciences, Beijing 100049, China
[c] Key Laboratory of Digital Earth, Institute of Remote Sensing and Digital Earth, Chinese Academy of Sciences, Beijing 100101, China
[d] Department of Geography and Program in Planning, University of Toronto, 100 St. George St., Toronto, ON M5S 3G3, Canada
[e] Faculty of Land and Food Systems, University of British Columbia, Vancouver, BC, Canada
[f] School of Geography and Earth Sciences and McMaster Centre for Climate Change, McMaster University, Hamilton, Ontario, Canada
[g] Department of Earth & Environmental Engineering, Columbia University, 500 W 120th St., New York, NY 10027, USA

ARTICLE INFO

Article history:
Received 5 November 2014
Received in revised form 16 January 2016
Accepted 22 January 2016
Available online 5 February 2016

Keywords:
Remote sensing
Phenology
MODIS
Needleleaf forests
NDVI
EVI

ABSTRACT

Plant phenology plays a significant role in regulating carbon sequestration period of terrestrial ecosystems. Remote sensing of land surface phenology (LSP), i.e., the start and the end of the growing season (SOS and EOS, respectively) in evergreen needleleaf forests is particularly challenging due to their limited seasonal variability in canopy greenness. Using 107 site-years of CO_2 flux data at 14 evergreen needleleaf forest sites in North America, we developed a new model to estimate SOS and EOS based entirely on the Moderate Resolution Imaging Spectroradiometer (MODIS) data. We found that the commonly used vegetation indices (VI), including the normalized difference vegetation index (NDVI) and enhanced vegetation index (EVI), were not able to detect SOS and EOS in these forests. The MODIS land surface temperature (LST) showed better performance in the estimation of SOS than did a single VI. Interestingly, the variability of LST (i.e., the coefficient of variation, CV_LST) was more useful than LST itself in detecting changes in forest LSP. Therefore, a new model using the product of VI and CV_LST was developed and it significantly improved the representation of LSP with mean errors of 11.7 and 5.6 days for SOS and EOS, respectively. Further validation at five sites in the Long Term Ecological Research network (LTER) using camera data also indicated the applicability of the new approach. These results suggest that temperature variability plays a previously overlooked role in phenological modeling, and a combination of canopy greenness and temperature could be a useful way to enhance the estimation of evergreen needleleaf forest phenology of future ecosystem models.

© 2016 Elsevier Inc. All rights reserved.

1. Introduction

Phenology is one of the most important controls of interannual variability of gross/net ecosystem productivity (GEP/NEP) (Fu, Campioli, Vitasse, et al., 2014; Gonsamo, Chen, Wu, & Dragoni, 2012; Jin et al., 2013; Richardson et al., 2013; Sakamoto, Gitelson, & Arkebauer, 2013; Wu, Chen, Black, et al., 2013; Zhang, Cheng, Lyapustin, Wang, Gao, et al., 2014; Zhang, Cheng, Lyapustin, Wang, Xiao, et al., 2014). Therefore, increasing efforts have been made to model phenological variations using remote sensing data, which is considered as the most convenient and efficient way in understanding vegetation dynamics at regional to global scales (Hmimina et al., 2013; Melaas, Richardson, et al., 2013; White et al., 2009; Wu, Hou, Peng, Gonsamo, & Xu, 2016).

Growing season phenology from remote sensing is determined by detecting the seasonal dynamics of vegetation greenness using spectral signals from sensors onboard satellite platforms (Melaas, Friedl, & Zhu, 2013; Sonnentag et al., 2012; Wu, Gonsamo, Gough, Chen, & Xu, 2014). A widely used remote sensing-based phenological data source is the Moderate Resolution Imaging Spectroradiometer (MODIS), and several vegetation indices (VIs) were reported to have potential in indicating phenological transitions (Friedl et al., 2010; Ganguly, Friedl, Tan, Zhang, & Verma, 2010; Gonsamo, Chen, Price, Kurz, & Wu, 2012; Hmimina et al., 2013; Jin & Eklundh, 2014; Sakamoto et al., 2010; Xiao, Hagen, Zhang, Keller, & Moore, 2006; Zhang et al., 2003). For example, both the normalized difference vegetation index (NDVI, Tucker & Sellers, 1986) and the enhanced vegetation index (EVI, Huete et al.,

* Corresponding authors.
E-mail addresses: hefery@163.com (C. Wu), pengdl@radi.ac.cn (D. Peng).

http://dx.doi.org/10.1016/j.rse.2016.01.021
0034-4257/© 2016 Elsevier Inc. All rights reserved.

2002) are extensively used in reconstructing phenological transitions for various plant functional types, including forests, grasslands, and croplands (Hmimina et al., 2013; Jeganathan, Dash, & Atkinson, 2014; Wu et al., 2014; Zhang & Goldberg, 2011; Zhang et al., 2003). One of the most widely used algorithm to model phenological changes is to detect the local maxima/minima in the rate of change of curvature (i.e., local inflection points) in a fitted curve from time-series of remote sensing signals (Friedl et al., 2010; Ganguly et al., 2010; Zhang et al., 2003; Zhang, Friedl, & Schaaf, 2006). More recently, signals from seasonal (e.g., spring and autumn) mean VIs have been shown to be useful in detecting changes in land surface phenology (Wu et al., 2014).

Forests are the most important ecosystems in terrestrial carbon budget (Pan et al., 2011), and their phenology consequently has played a significant role in explaining interannual variability of NEP (Richardson et al., 2010, 2013; Wu, Chen, Black, et al., 2013). However, there are several challenges in modeling forest phenology from remote sensing data. The most confounding issue related to phenological modeling to date is the limited potential of VIs to estimate LSP in needleleaf forests because of small seasonal VI variation (Guyon et al., 2011; Hufkens et al., 2012; Melaas, Friedl, et al., 2013; Shen, Tang, Desai, et al., 2014). For example, Hmimina et al. (2013) showed that MODIS is unable to accurately infer phenological patterns for needleleaf forests. In comparison, with evident variations in canopy greenness, changes in phenology of deciduous forests is much easier to detect (Garrity, Maurer, Mueller, Vogel, & Curtis, 2011; Gonsamo, Chen, Price, et al. 2012; Luo, Chen, Wang, Xu, & Tian, 2014; Melaas, Richardson, et al., 2013; Melaas, Friedl, et al., 2013; Ryu, Lee, Jeon, Song, & Kimm, 2014; Wu et al., 2014). This problem becomes more severe for detecting the end of growing season (EOS) in autumn since this period sustains a much longer and slower change of canopy greenness compared to that of the start of growing season (SOS) in spring (Richardson et al., 2013; White, Pontius, & Schaberg, 2014; Wu et al., 2014).

Remote sensing of phenology using time-series of VIs is based on the intra-annual changes of canopy greenness. Essentially, this is an external expression of plant dynamics to plant growth determinants (e.g., temperature, soil water content) which strongly regulate the growth dynamics of boreal and temperate forests. For example, temperature has been long recognized as a main driver of plant growth, and spring air temperature was found to trigger the recovery of photosynthesis in most boreal and temperate ecosystems (Barr, Black, & McCaughey, 2009; Chen et al., 2003; Suni, Berninger, Vesala, et al., 2003). Apart from temperature itself, it is also possible that the temperature variability may have an unrecognized role on phenology and its modeling. For example, Wheeler, Craufurd, Ellis, Porter, and Prasad (2000) showed a strong evidence for the importance of variability in temperature, independent of any substantial changes in mean seasonal temperature, for the yield of annual crops. In particular, seed yields are particularly sensitive to brief episodes of hot temperatures if these coincide with critical stages of crop development. Furthermore, Reyer et al. (2013) indicates that distinguishing between impacts of changing mean climatic conditions and changing climatic variability on terrestrial ecosystems is generally underrated in current studies. They found that phenology is largely affected by changing mean climate but also that impacts of climatic variability are much less studied. The problem is that how temperature, in particularly remote sensing based observations (e.g., MODIS Land Surface Temperature product (LST)), can be incorporated to better depict evergreen needleleaf forest phenology? For example, Gonsamo, Chen, Wu, et al. (2012) has shown that the combination of remotely sensed VI and LST is a good indicator of the start and end of net positive carbon uptake period of broadleaf forests. Therefore, using continuous CO_2 flux measurements at 14 evergreen needleleaf forests and five additional PhenoCam sites in North America, this study explores the potential of a new model that incorporates MODIS VIs and LST products to estimate the boreal and temperate evergreen needleleaf forest phenology. The questions we address include: (i) can MODIS NDVI and EVI be used to model SOS and EOS of needleleaf forests?; (ii) Is temperature variability more important than average temperature itself in detecting plant greenness dynamics?; (iii) if so, does the combination of MODIS VI and LST improve the accuracy of modeled SOS and EOS?

2. Methods

2.1. Flux sites and CO_2 flux data

To support the phenological analysis of this study, we used CO_2 flux data from 14 evergreen needleleaf forest (ENF) flux tower sites in North America from the AmeriFlux and Canadian Carbon Program (CCP) formerly known as Fluxnet-Canada networks with at least 5 years of complete data with less than 20% gap-filled in each year (Fig. 1). Detailed descriptions of these sites are given in Table 1.

Half-hourly CO_2 fluxes were continuously measured at each site using the eddy-covariance technique (Baldocchi et al., 2001). Regional flux networks adopt several standard procedures to partition the directly measured net ecosystem exchange (NEE) into gross primary productivity (GPP) and total ecosystem respiration (R_e). Because these study sites belong to two different regional flux networks within North America, gap-filling and NEE partitioning approach is different. For CCP sites, the NEE portioning was conducted using the network's standard approaches described in Barr et al. (2013). For the AmeriFlux sites, the Artificial Neural Network (ANN) method (Papale & Valentini, 2003) and/or the Marginal Distribution Sampling (MDS) method (Reichstein et al., 2005) were adopted to conduct level-4 products that contain gap-filled and u* filtered records of CO_2 fluxes at varying time intervals. Though various flux networks applied different decomposition techniques to flux data, they generally have a negligible impact on modeled GPP (Desai et al., 2008; Wu, Chen, Black, et al., 2013; Wu, Chen, Desai, Lafleur, & Verma, 2013).

2.2. Canopy phenology from PhenoCam network

Digital repeat photography makes consistent visual assessment of phenology possible over broad geographic ranges and has played an important role in phenological analysis recently (Sonnentag et al., 2012; Klosterman et al., 2014). The PhenoCam network is a continental-scale phenological observatory, spanning a wide range of biogeoclimatic zones and vegetation types, across the northeastern US and adjacent Canada (Imagery and data products are available at the PhenoCam website http://phenocam.sr.unh.edu/webcam/). Over the thirteen geographically distinct research sites in PhenoCam network, we identified five sites dominated by the evergreen forests species that are suitable for our analysis (Table 2).

2.3. MODIS data

In this study, we used two MODIS land surface products acquired from the Oak Ridge National Laboratory Distributed Archive Center (DAAC) website (http://daac.ornl.gov/cgi-bin/MODIS/GR_col5_1/mod_viz.html). The first product was the 8-day Terra MODIS Surface Reflectance product (MOD09A1, 500 m, quality control was done for cloud, view angle, and aerosol), which was used to compute NDVI and EVI in this study. For each site, both NDVI and EVI were extracted from 3×3 MODIS pixels centered on the flux tower similar to the approach used by Sims et al. (2008). The 3×3 MODIS pixels method was also confirmed to represent each site with respect to both footprints (flux-tower fetch) (~1 km) and land cover (Chen et al., 2011).

The second product is the MODIS 8-day Land Surface Temperature (LST) and Emissivity product (MOD11A2, 1 km) derived by applying the generalized split-window algorithm. In the split-window algorithm, emissivity in spectral bands 31 and 32 is estimated from land cover types, and atmospheric column water vapor and lower boundary air

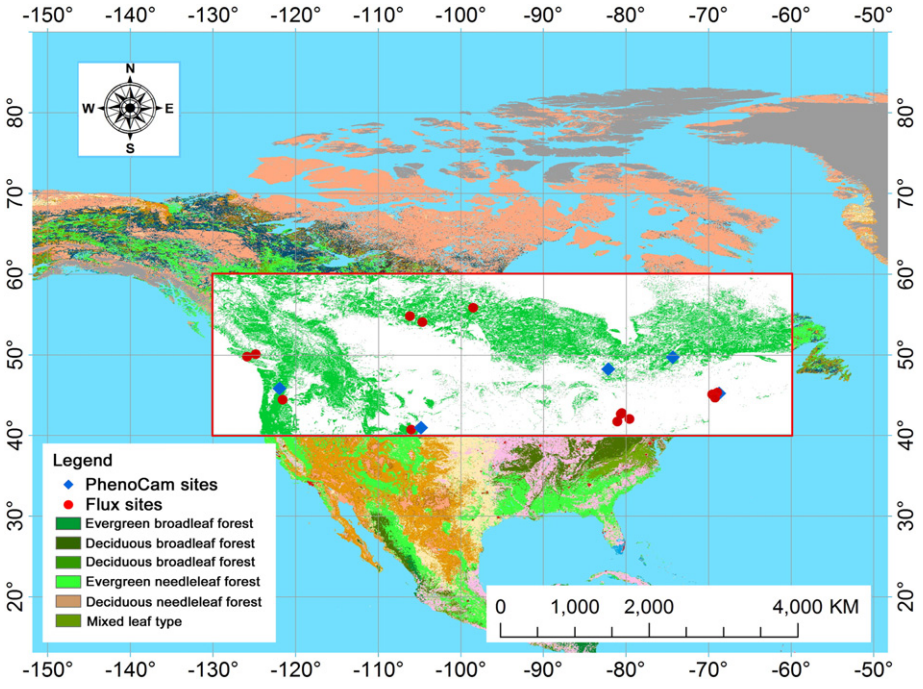

Fig. 1. Spatial distribution of the 14 flux tower sites (●) and 5 PhenoCam sites (◆) in North America used in this study.

surface temperature are separated into tractable sub-ranges for optimal retrieval (Wan, 2008).

2.4. Determination of land surface phenology from daily GPP

We adopted a negative exponential model, using polynomial regression and weights computed from the Gaussian density function to derive smoothed curves for daily GPP observations for each site. The SOS and EOS were then defined as the dates when smoothed curves of daily GPP first and last reached 10% of the seasonal maximum GPP, respectively (Wu et al., 2012). Compared with most contemporary methods (e.g., 0.5–2 g C/m^2/d in Richardson et al., 2010), a varied GPP threshold derived SOS and EOS effectively allows for variation in phenological events to be quantified and compared both inter-annually and spatially (Wu et al., 2012; Wu, Chen, Black, et al., 2013; Wu, Chen, Desai, et al., 2013). Fig. 2 illustrates the schematic example of the phenological transition dates from daily GPP data at SK-OBS site for year 2005.

We used seasonal mean seasonal VIs for the estimation SOS and EOS in this study since it has been shown that this approach might be more useful than the inflection points in indicating SOS and EOS (Wu et al., 2014). The modeling strategy was that we correlated SOS with spring data (VI and LST in March–May) and EOS with autumn data from September to November. Then, based on the correlations between SOS (and EOS) and VI, and LST, we proposed that a combination of VI and LST could improve the modeled SOS (and EOS). To investigate the potential of a single VI in modeling SOS and EOS, we used both NDVI and EVI. For LST, we calculated the mean seasonal data of LST and its variability, i.e., coefficient of variation (CV_LST, %), because it has a better potential to indicate variability when the mean temperature can vary substantially among sites from different regions.

2.5. Phenological transitions from PhenoCam observations

To quantify phenological status of the forest canopy over time, green chromatic coordinate (GCC) within the region of interest (ROI) for each image from average red (R), green (G), and blue (B) pixel digital numbers (DNs) were calculated, where GCC is defined as

$$GCC = G/(R + G + B). \quad (1)$$

According to previous studies (Klosterman et al., 2014; Zhang et al., 2003), we used a sigmoid-based method to fit the time-series of GCC

Table 1
Descriptions of flux sites in this study.

Site_ID	Site_name	Latitude (°)	Longitude (°)	Altitude (m)	Data period	References
SK-OBS	Sask.- SSA Old Black Spruce	53.99	−105.12	629	2000–2010	Barr et al. (2004)
ON-TP39	Turkey Point 1939 Plantation White Pine	42.71	−80.36	184	2003–2013	Arain, Yaun, and Black (2006)
ON-TP74	Turkey Point 1974 Plantation White Pine	42.71	−80.35	184	2003–2007	Arain et al. (2006)
ON-TP89	Turkey Point 1989 Plantation White Pine	42.77	−80.46	212	2003–2007	Arain et al. (2006)
ON-TP02	Turkey Point 2002 Plantation White Pine	42.66	−80.56	265	2003–2007	Arain et al. (2006)
SK-OJP	SSA Old Jack Pine	53.92	−104.69	579	2000–2008	Barr et al. (2004)
MB-OBS	BOREAS NSA — Old Black Spruce	55.88	−98.48	259	2000–2007	Dunn, Barford, Wofsy, Goulden, and Daube (2007)
BC-DF00	Clearcut Douglas-fir stand	49.87	−125.29	300	2002–2009	Jassal, Black, Spittlehouse, Brümmer, and Nesic (2009)
BC-DF49	British Columbia — 1948 Douglas-fir stand	49.87	−125.33	300	2002–2009	Jassal et al. (2009)
US-HO1	Howland Forest (main tower)	45.20	−68.74	60	2000–2008	Hollinger et al. (2004)
US-HO2	Howland Forest (west tower)	45.21	−68.75	91	2000–2009	Hollinger et al. (2004)
US-HO3	Howland Forest (harvest site)	45.21	−68.73	61	2004–2008	Hollinger et al. (2004)
US-NR1	Niwot Ridge Forest (LTER NWT1)	40.03	−105.55	3050	2000–2007	Monson et al. (2005)
US-ME2	Metolius-intermediate aged ponderosa pine	44.45	−121.56	1253	2002, 2004–2007	Thomas et al. (2009)

Table 2
Descriptions of PhenoCam sites in this study.

Sites	Latitude	Longitude	Elevation (m)	Data range	References
Chibougamau	49.69	−74.34	380	2008–2010	Bergeron, Margolis, Coursolle, and Giasson (2008)
Groundhog	48.22	−82.16	350	2008–2011	McCaughey, Pejam, Arain, and Cameron (2006)
Howland (main tower)	45.20	−68.74	60	2010–2012	Hollinger et al. (2004)
Niwot Ridge Forest (LTER NWT1)	40.03	−105.55	3050	2008–2011	Monson et al. (2005)
Wind River	45.82	−121.95	371	2011	Wharton, Falk, Bible, Schroeder, and Paw (2012)

(see Eq. (2)), and to calculate the SOS and EOS as local extrema in the rate of change of curvature k in Eq. (3) (Fig. 3):

$$f(t) = m_1 + (m_2 - m_7 t) \times \left[\frac{1}{1 + \exp((m_3 - t)/m_4)} - \frac{1}{1 + \exp((m_5 - t)/m_6)}\right] \quad (2)$$

$$k = \frac{f''(t)}{\left(1 + (f'(t))^2\right)^{\frac{3}{2}}}. \quad (3)$$

2.6. Analysis strategy

To compare the performance of single seasonal VI (both NDVI and EVI), LST and its variability, and the new model (i.e., NDVI/EVI × CV_LST) in the estimation of SOS and EOS, we used least-squares linear regression to calculate root mean square error (RMSE), coefficients of determination (R^2) and p-value. To determine the correctness of modeled SOS and EOS from NDVI/EVI × CV_LST for flux and PhenoCam sites, we used the leave-one-out cross-validation approach (Gonsamo, Chen, Wu, et al., 2012; Wu et al., 2014). We further used the analysis of variance (ANOVA) technique (Duncan's multiple range test, $p = 0.05$) to analyze whether the reduction in residual sum of squares between these models is statistically significant or not with SPSS software (SPSS v19.0, IBM Corp, 2010).

3. Results

3.1. Temporal patterns of GPP, NDVI/EVI and monthly air temperature

We analyzed the temporal patterns of GPP, NDVI, EVI and monthly air temperature (T_a) for each flux site (Fig. 4). We observed that T_a increased over time in spring and decreased in autumn. Monthly GPP exhibited the same trend. Though canopy NDVI and EVI had a small dynamic range for evergreen species, we still showed a clear pattern for both NDVI and EVI. Overall, all four variables followed the same temporal pattern, suggesting that at the monthly temporal scale, GPP is quite sensitive to both T_a and vegetation indices and there does not seem to have an evident time lag at monthly or seasonal temporal scale between productivity and temperature.

3.2. Modeling SOS from VI, LST and models

We compared the performance of remote sensing based estimates of SOS with corresponding reference measure from GPP based phenology estimates. Table 3 shows the relationships between SOS and single VI, LST (CV_LST) in spring and the products of NDVI/EVI × LST/CV_LST for each site. Temperature has been suggested as an important controller of plant phenology and this was confirmed in our analysis. To propose a model using entirely satellite data, the MODIS LST product was used as a substitute of air temperature. Apart from LST, we also introduced the variability of LST (its coefficient of variation, CV_LST) for phenological modeling.

NDVI was correlated with SOS for the ON-TP39 ($R^2 = 0.63$, $p = 0.003$) and US-NR1 ($R^2 = 0.67$, $p = 0.012$) sites. EVI demonstrated relatively low potential that EVI was not significantly correlated with SOS for any sites. For spring LST-based SOS estimates, statistically significant correlations were found for seven sites (SK-OBS, ON-TP39, SK-OJP, MB-OBS, BC-DF00, US-HO1 and US-HO2) with the highest correlation for ON-TP39 with an R^2 of 0.64 ($p = 0.003$). CV_LST was demonstrated to have an improved potential as an indicator of SOS, with significant correlations found for ten sites (SK-OBS, ON-TP39, ON-TP74, ON-TP89, SK-OJP, MB-OBS, BC-DF00, BC-DF49, US-HO1 and US-HO2). Basically, the product of NDVI/EVI and LST did not have high potential for SOS

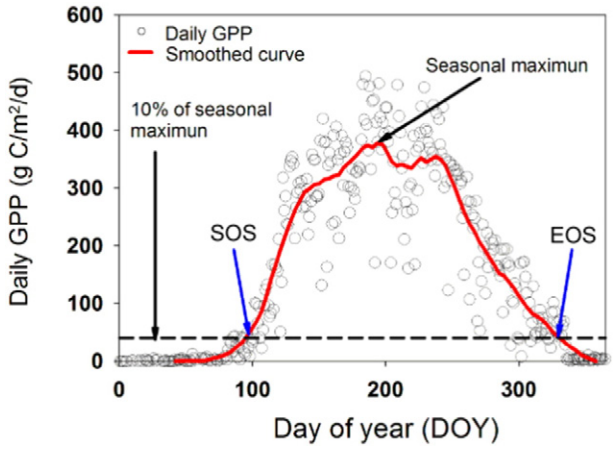

Fig. 2. The schematic representation for calculating land surface phenology (start and end of growing season, SOS and EOS, respectively) from daily gross primary productivity (GPP) at SK-OBS in 2005.

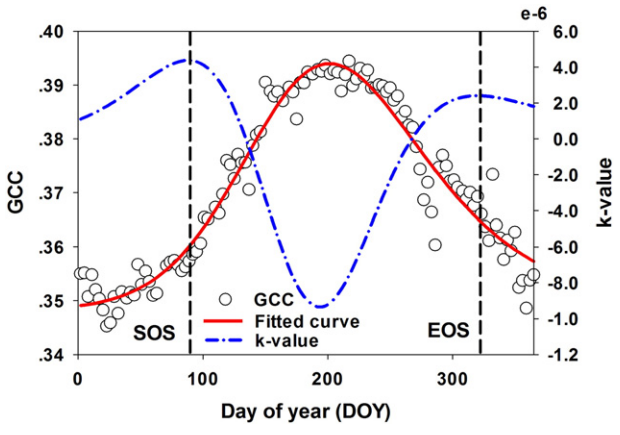

Fig. 3. Illustration of determining the start and end of growing season (SOS and EOS) from observed green chromatic coordinate (GCC) using camera data at US-HO1 in 2011. Local extrema in the rate of change of curvature k were used to identify SOS and EOS in spring and autumn, respectively.

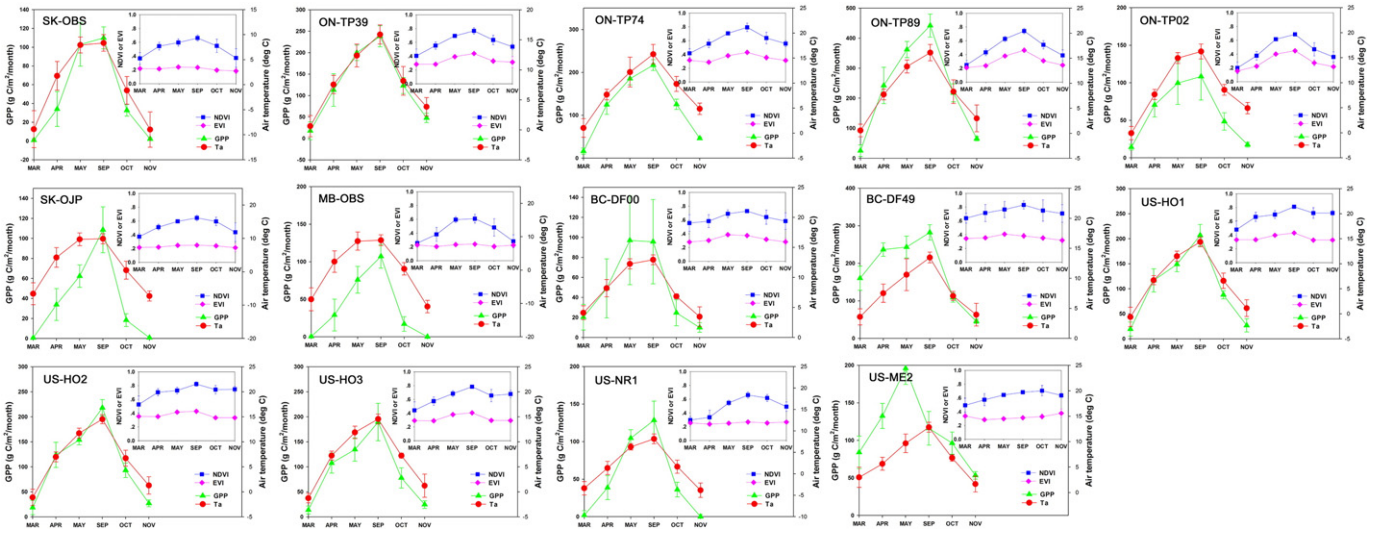

Fig. 4. Temporal patterns of gross primary productivity (GPP), air temperature (T_a), normalized difference vegetation index (NDVI) and enhanced vegetation index (EVI) for each flux site. Error bars represent the standard deviations over the study period for each site.

modeling that we found that NDVI × LST provided significant SOS estimates at three sites (ON-TP39, MB-OBS and US-NR1) while EVI × LST can only predict reliable SOS at MB-OBS site.

We found that the product of NDVI × CV_LST and EVI × CV_LST can improve the accuracy of modeled SOS compared to a single VI-based or VI × LST approaches for most sites. NDVI × CV_LST significantly correlated with SOS for the SK-OBS, ON-TP39, ON-TP74, SK-OJP, MB-OBS, BC-DF00, BC-DF49, US-HO1 and US-HO3 sites. In particular, the highest correlation was found for the US-HO3 and BC-DF00 sites using NDVI × CV_LST (both $R^2 = 0.86$, $p < 0.001$). EVI × CV_LST also exhibited relatively high potential as an indicator of SOS with significant relationships found for the SK-OBS, ON-TP39, ON-TP74, ON-TP89, SK-OJP, MB-OBS, BC-DF00, BC-DF49, US-HO1 and US-HO2 sites. The highest R^2 of 0.88 ($p = 0.019$) was observed between EVI × CV_LST and SOS for ON-TP74.

3.3. Modeling EOS from VI, LST and models

Table 4 shows the predictive strength of indicators and models for EOS modeling. For EOS, NDVI only had significantly correlation at two sites: ON-TP74 ($R^2 = 0.85$, $p = 0.025$) and US-NR1 ($R^2 = 0.54$, $p = 0.032$) while EVI showed a comparable potential with significant correlations also for two sites, namely ON-TP39 ($R^2 = 0.61$, $p = 0.004$), SK-OJP ($R^2 = 0.50$, $p = 0.034$) and BC-DF00 ($R^2 = 0.36$, $p = 0.085$). We found that the AVE_LST was significantly correlated with EOS for the ON-TP39 ($R^2 = 0.46$, $p = 0.023$), US-HO1 ($R^2 = 0.45$, $p = 0.049$) and

Table 3
The predicting performances (in terms of R-square) of start of growing season (SOS) using NDVI, EVI, LST, CV_LST, VI × LST and VI × CV_LST for each site. LST is the man average of LST in Mar–May. NS represents that the correlation is not significant. * and ** denote correlation significant at the 0.05 and 0.01 p-value level, respectively. Bold font shows the highest correlation among all indicators. For regression equations, Y and x indicate SOS and model variable, respectively.

Site_ID	NDVI	EVI	LST	CV_LST	NDVI × LST	EVI × LST	NDVI × CV_LST	EVI × CV_LST
SK-OBS	NS	NS	$Y = -2.7x + 864$, $R^2 = 0.56^{**}$	$Y = 3.9\times + 83$, $R^2 = 0.61^{**}$	NS	NS	$Y = 6.0x + 85.9$, $R^2 = 0.61^{**}$	**$Y = 15.3x + 85.1$, $R^2 = 0.62^{**}$**
ON-TP39	$Y = -157x + 171$, $R^2 = 0.63^{*}$	NS	$Y = -3.3x + 1039$, $R^2 = 0.64^{**}$	$Y = 10.3x + 48$, $R^2 = 0.62^{**}$	$Y = -0.53x + 168$, $R^2 = 0.67$	NS	**$Y = 34x + 17.3$, $R^2 = 0.64^{**}$**	$Y = 36x + 43.3$, $R^2 = 0.63^{**}$
ON-TP74	NS	NS	NS	$Y = 4.2x + 69.3$, $R^2 = 0.80^{*}$	NS	NS	$Y = 13x + 61.8$, $R^2 = 0.87^{*}$	**$Y = 22x + 58.5$, $R^2 = 0.88^{*}$**
ON-TP89	NS	NS	NS	$Y = 21.2x - 2.9$, $R^2 = 0.78^{*}$	NS	NS	NS	**$Y = 99x - 32.3$, $R^2 = 0.80^{*}$**
ON-TP02	NS	NS	NS	NS	NS	NS	NS	NS
SK-OJP	NS	NS	$Y = -3.1x + 978$, $R^2 = 0.50^{*}$	$Y = 4.8x + 91.2$, $R^2 = 0.52^{*}$	NS	NS	$Y = 11x + 75.7$, $R^2 = 0.50^{*}$	**$Y = 29x + 69.4$, $R^2 = 0.53^{*}$**
MB-OBS	NS	NS	$Y = -2.8x + 879$, $R^2 = 0.52^{*}$	$Y = -9.5x + 150$, $R^2 = 0.56^{*}$	$Y = -0.55x + 165$, $R^2 = 0.44^{*}$	$Y = -2.3x + 243$, $R^2 = 0.49^{*}$	$Y = -19x + 141$, $R^2 = 0.57^{*}$	**$Y = -50x + 158$, $R^2 = 0.58^{*}$**
BC-DF00	NS	NS	$Y = -5.2x + 1558$, $R^2 = 0.55^{*}$	$Y = -36x + 175$, $R^2 = 0.74^{**}$	NS	NS	**$Y = -37x + 139$, $R^2 = 0.86^{**}$**	$Y = -122x + 179$, $R^2 = 0.80^{**}$
BC-DF49	NS	NS	NS	$Y = -8.9x + 37$, $R^2 = 0.52^{*}$	NS	NS	$Y = -25x + 56.7$, $R^2 = 0.58^{*}$	**$Y = -53x + 65.5$, $R^2 = 0.63^{**}$**
US-HO1	NS	NS	$Y = -3x + 939$, $R^2 = 0.55^{*}$	$Y = 9.2x + 56.4$ $R^2 = 0.60^{**}$	NS	NS	$Y = 15.7x + 55.7$, $R^2 = 0.66^{**}$	**$Y = 74.4x + 55.1$, $R^2 = 0.72^{**}$**
US-HO2	NS	NS	$Y = -3.1x + 971$, $R^2 = 0.43^{*}$	$Y = 9.3x + 54$, $R^2 = 0.41^{*}$	NS	NS	NS	**$Y = 24x + 56.0$, $R^2 = 0.57^{*}$**
US-HO3	NS	NS	NS	NS	NS	NS	**$Y = 13x + 65.6$, $R^2 = 0.86^{*}$**	NS
US-NR1	$Y = -127x + 148$, $R^2 = 0.67^{*}$	NS	NS	NS	**$Y = -0.45x + 148$, $R^2 = 0.86^{**}$**	NS	NS	NS
US-ME2	NS	NS	NS	NS	NS	NS	NS	NS

Table 4
The predicting performances (in terms of R-square) of end of growing season (EOS) using NDVI, EVI, LST, CV_LST, VI × LST and VI × CV_LST for each site. LST is the man average of LST in Sep.-Nov. NS represents that the correlation is not significant. * and ** denote correlation significant at the 0.05 and 0.01 p-value level, respectively. Bold font shows the highest correlation among all indicators. For regression equations, Y and x indicate EOS and model variable, respectively.

Site_ID	NDVI	EVI	LST	CV_LST	NDVI × LST	EVI × LST	NDVI × CV_LST	EVI × CV_LST
SK-OBS	NS	NS	NS	NS	NS	NS	NS	NS
ON-TP39	NS	$Y = -103x + 368$, $R^2 = 0.61^*$	NS	$Y = -9.2x + 359$, $R^2 = 0.46^*$	NS	$Y = -0.36x + 366$, $R^2 = 0.61^*$	$Y = -13.7x + 358$, $R^2 = 0.57^*$	**$Y = -18x + 351$, $R^2 = 0.67^*$**
ON-TP74	**$Y = -25x + 350$, $R^2 = 0.85^*$**	NS	NS	NS	$Y = -0.08x + 349$, $R^2 = 0.77^*$	NS	NS	NS
ON-TP89	NS	NS	NS	NS	NS	NS	NS	NS
ON-TP02	NS	NS	NS	NS	NS	NS	NS	NS
SK-OJP	NS	$Y = -177x + 344$, $R^2 = 0.50^*$	NS	NS	NS	$Y = -0.6x + 341$, $R^2 = 0.46^*$	$Y = -7.4x + 318.4$, $R^2 = 0.53^*$	**$Y = -20.5x + 323$, $R^2 = 0.72^{**}$**
MB-OBS	NS	NS	NS	NS	NS	NS	NS	NS
BC-DF00	NS	NS	NS	NS	NS	**$Y = 1.4x + 174$, $R^2 = 0.44^*$**	NS	NS
BC-DF49	NS	NS	NS	NS	NS	NS	$Y = -16x + 377$, $R^2 = 0.38^*$	**$Y = -34x + 377$, $R^2 = 0.40^*$**
US-HO1	NS	NS	$Y = 2.1x - 277$, $R^2 = 0.45^*$	$Y = -6x + 345$, $R^2 = 0.47^*$	NS	NS	**$Y = -6x + 341$, $R^2 = 0.63^*$**	NS
US-HO2	NS	NS	NS	$Y = -12x + 363$, $R^2 = 0.60^*$	NS	NS	$Y = -12x + 357$, $R^2 = 0.60^*$	**$Y = -24x + 355$, $R^2 = 0.63^*$**
US-HO3	NS	NS	NS	NS	NS	NS	NS	NS
US-NR1	$Y = 116x + 239$, $R^2 = 0.54^*$	NS	$Y = 5.1x - 1118$, $R^2 = 0.82^{**}$	$Y = -11x + 345$, $R^2 = 0.65^*$	$Y = 0.4x + 239$, $R^2 = 0.58^*$	NS	$Y = -22x + 351$, $R^2 = 0.61^*$	**$Y = -47x + 349$, $R^2 = 0.88^{**}$**
US-ME2	NS	NS	NS	NS	NS	NS	NS	NS

US-NR1 ($R^2 = 0.82$, $p = 0.002$) sites. Compared with AVE_LST, CV_LST showed high potential as an indicator of EOS with significant relationships found for the US-HO1 ($R^2 = 0.47$, $p = 0.039$), US-HO2 ($R^2 = 0.60$, $p = 0.005$) and US-NR1 ($R^2 = 0.65$, $p = 0.016$) sites.

We found that NDVI × LST can predict EOS at two sites that were significantly correlated with observations (ON-TP74, $R^2 = 0.77$, $p = 0.048$, and US-NR1, $R^2 = 0.58$, $p = 0.027$). In comparison, three sites were identified to have significant EOS estimates using EVI × LST (ON-TP39, $R^2 = 0.61$, $p = 0.004$, SK-OJP, $R^2 = 0.46$, $p = 0.048$, BC-DF00, $R^2 = 0.44$, $p = 0.044$). Better estimates of SOS and EOS were observed with NDVI/EVI × CV_LST than using single VI, LST, and CV_LST. NDVI × CV_LST was significantly correlated with EOS at six sites, including ON-TP39 ($R^2 = 0.57$, $p = 0.007$), SK-OJP ($R^2 = 0.53$, $p = 0.026$), BC-DF49 ($R^2 = 0.38$, $p = 0.044$), US-HO1 ($R^2 = 0.63$, $p = 0.016$), US-HO2 ($R^2 = 0.60$, $p = 0.008$) and US-NR1 ($R^2 = 0.61$, $p = 0.022$). For EVI × CV_LST, there were five sites showing significant relationships, namely ON-TP39 ($R^2 = 0.67$, $p = 0.002$), SK-OJP ($R^2 = 0.72$, $p = 0.004$), BC-DF49 (R2 = 40, $p = 0.039$), US-HO2 ($R^2 = 0.63$, $p = 0.013$) and US-NR1 ($R^2 = 0.88$, $p < 0.001$).

3.4. Predictive capability of NDVI/EVI × CV_LST in modeling SOS and EOS

To show the predictive capability of NDVI/EVI × CV_LST in modeling SOS and EOS, we used the leave-one-out cross validation for sites where significant correlations were found. Strong correlation was found between observed and modeled SOS for ten sites using NDVI × CV_LST with overall R^2 of 0.85 ($p < 0.001$) and RMSE of 10.6 days (Fig. 5). Comparable results were also found with EVI × CV_LST ($R^2 = 0.77$, $p < 0.001$, RMSE = 13.4 days). For EOS, NDVI × CV_LST produced quite promising results for six sites with R^2 of 0.89 ($p < 0.001$) and RMSE of 5.7 days for the overall dataset (Fig. 6a). EVI × CV_LST showed comparable result with R^2 of 0.91 ($p < 0.001$) and RMSE of 5.4 days.

3.5. Validation at PhenoCam sites and phenology mapping

We also validated our approach at PhenoCam sites using EVI × CV_LST and the results were also promising (Fig. 7). An R^2 of 0.59 ($p = 0.006$) was found between ground observed and modeled SOS and the respective RMSE was 15.7 days. Similarly, predicted EOS was also significantly correlated with ground observations ($R^2 = 0.60$,

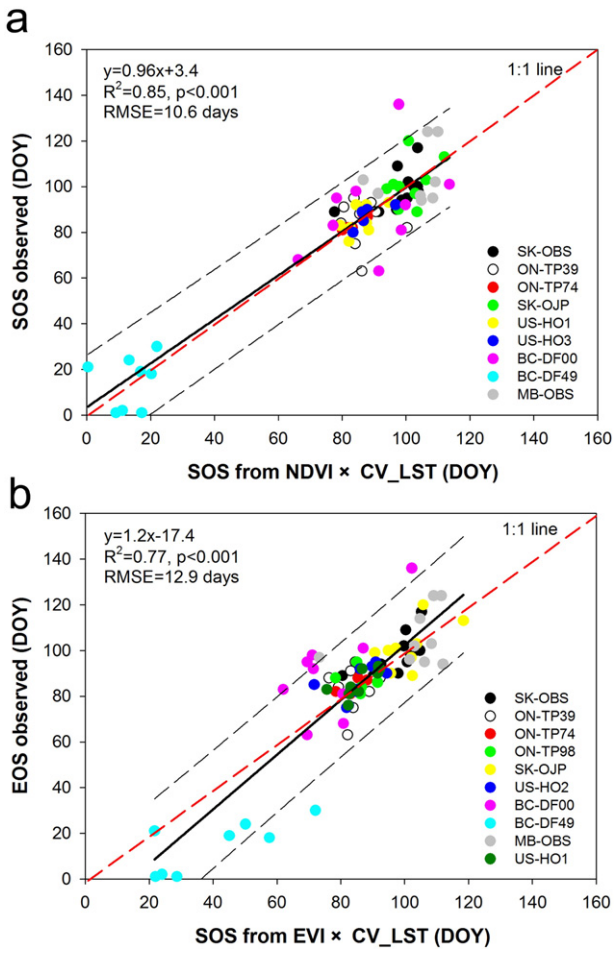

Fig. 5. Comparison between observed start of the growing season (SOS) and model outputs from (a) the product of normalized different vegetation index (NDVI) and the coefficient of variation of land surface temperature (LST) (i.e., NDVI × CV_LST) and (b) the product of enhanced vegetation index (EVI) and CV_LST (i.e., EVI × CV_LST) at sites for which significant correlations were observed (see Table 3).

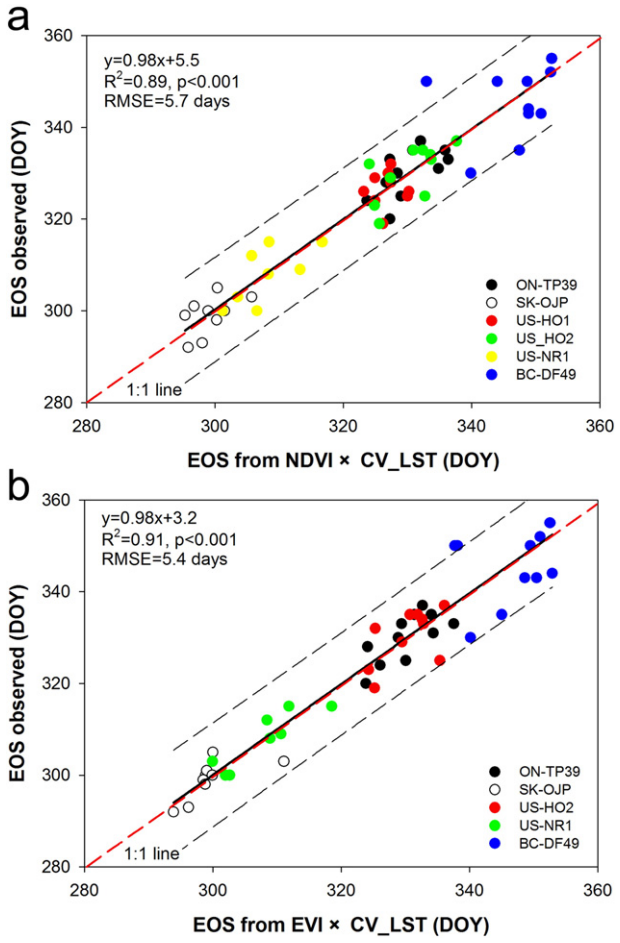

Fig. 6. Comparison between observed end of the growing season (EOS) and model outputs from (a) the product of normalized different vegetation index (NDVI) and the coefficient of variation of land surface temperature (LST) (i.e., NDVI × CV_LST) and (b) the product of enhanced vegetation index (EVI) and CV_LST (i.e., EVI × CV_LST) at sites for which significant correlations were observed (see Table 4).

p = 0.004, RMSE = 15.9 days). With the good results from two combined datasets, we mapped the SOS and EOS using MODIS EVI and LST over the study area in 2013 (Fig. 8). Overall, the modeled SOS was in the range between DOY 40 and 160 and there was an evident increase trend along the latitude gradient. Mountainous areas in west regions

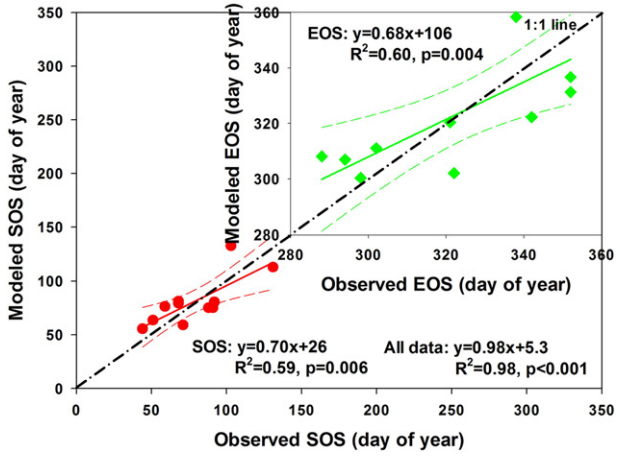

Fig. 7. Comparison between observed and modeled land surface phenology at PhenoCam sites with EVI CV_LST using leave-one-out cross-validation approach. SOS (●) and EOS (◆) represent the start and end of growing season, respectively.

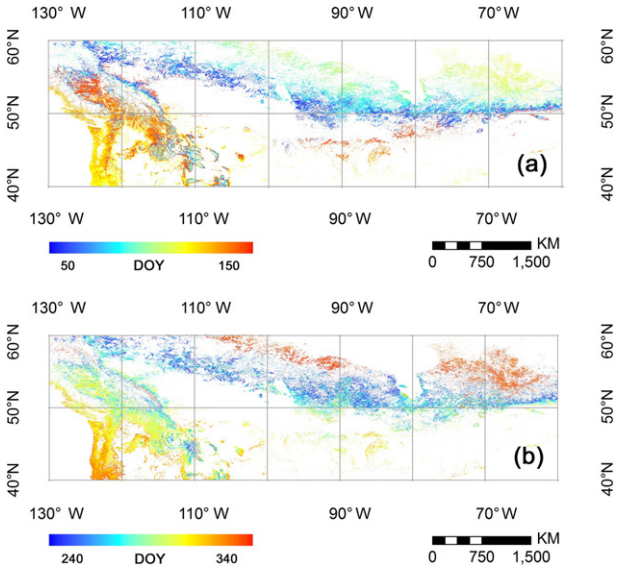

Fig. 8. Spatial distribution of the start (a) and end (b) of growing season from MODIS EVI and LST product over the study area in 2013.

had later SOS, probably due to high elevation and low temperature. Most pixels had EOS later than DOY of 220, and also exhibited a clear increase pattern from south to north and from east to west.

4. Discussion

4.1. The role of temperature variability in detecting plant phenology

Temperature has long been considered as the main determinant of phenology in many ecosystems (Chen et al., 2003; Garrity et al., 2011; Jeganathan et al., 2014; Richardson et al., 2013; Suni et al., 2003). Our results confirmed that temperature has evident influence on phenology, while the vegetation surface temperature as estimated by MODIS LST may be a proxy indicator of changes in land surface phenology. However, the potential of LST in indicating EOS in needleleaf forests is not evident as only two sites (US-HO1 and US-NR1) showed significant relationships with LST. This could be explained by abrupt change of vegetation in spring than autumn which can be captured well in MODIS LST which indicates both air and land surface skin temperature. One of the most useful finding of this study is that temperature variability is more important than average temperature itself in modeling phenology of needleleaf forests, as shown by improved correlation between CV_LST and SOS than between LST and SOS. This is applicable to EOS as well, but with poor performance. We showed that temperature variability (i.e., CV_LST) could provide a useful way for phenology modeling if we compare LST vs. CV_LST, NDVI × LST vs. NDVI × CV_LST and EVI × LST vs. EVI × CV_LST.

Modeling phenology from remote sensing is challenging and it is particularly difficult to develop a model that is universally workable in all situations. The practical way is to derive a model which is workable for most sites in this study. From Tables 3 and 4, we found that most bold font (i.e., best results) were in the model we newly proposed, and the new model is able to give much higher R^2 for most sites. The ANOVA technique using Duncan's multiple range test showed that CV_LST showed significant better results for phenology modeling than LST for both SOS and EOS (Fig. 9). Similarly, adding CV_LST to NDVI/EVI also significantly improved the accuracy of modeled SOS/EOS compared with either NDVI/EVI alone or NDVI/EVI × LST, suggesting a consistent helpful role of CV_LST played in modeling phenology.

The physical reasons for a better performance of temperature variability is not fully clear at present, but here we provided some clues

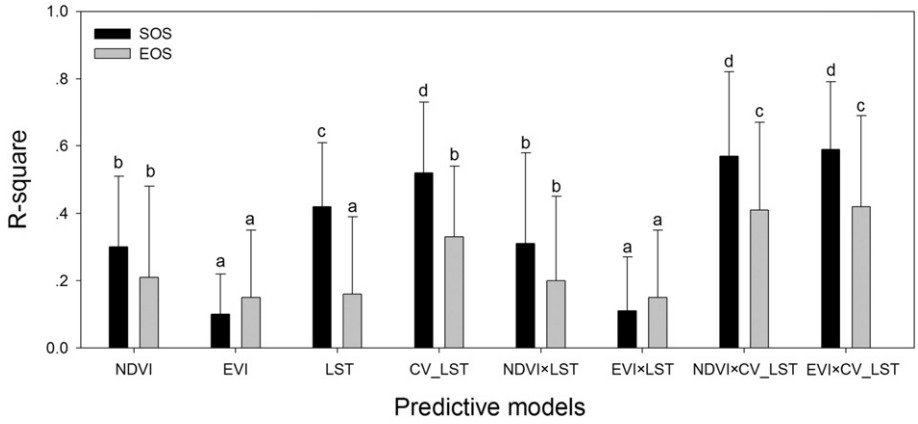

Fig. 9. Analysis of variance (ANOVA) technique using Duncan's multiple range test on the R-square between the start and end of growing season (SOS and EOS) using different predictive models. Different letters indicate significant level at $p = 0.05$.

for these results. We found a negative correlation between the CV_LST and the mean LST (Fig. 10a). It shows that higher CV_LST was associated with lower temperature in both spring and autumn, which in turn would delay SOS in spring and advance EOS in autumn with current knowledge (Black et al., 2000; Chen et al., 2003; Wu, Chen, Black, et al., 2013; Wu, Chen, Desai, et al., 2013). Therefore, the positive correlation between CV_LST and SOS and negative correlation between CV_LST and EOS were both consistent with previous understanding on the role of temperature on phenology. Second, relationship between CV_LST and mean LST exhibited a nonlinear form which indicates that they have different sensitivity at two sides. For example, CV_LST had a higher sensitivity at lower temperature end (it decreased quickly at low temperature) but lower sensitivity at the high end. Mean LST showed opposite patterns. This might be an important reason for the better performance of CV_LST for LSP modeling since it is more sensitive to low temperature change, which is typically the case at the SOS (temperature starts to increase) and EOS (temperature starts to decline) stages when temperature starts to change greatly. Finally, we further explored the correlation between LST/LST_CV and NDVI, because NDVI had been considered as a proxy of biomass and growth stages of vegetation (Fig. 10b, c). We found that LST_CV (both in spring and in autumn) had a better potential in capturing changes in NDVI, and this might be the underlying reason for a better performance in its modeling phenology across plant functional types.

4.2. Performances of NDVI and EVI

NDVI and EVI have been the most commonly used VIs in modeling land surface phenology over the past two decades (Gonsamo, Chen, Price, et al., 2012; Piao, Fang, Zhou, et al., 2006; Shen et al., 2014; Wu et al., 2014; Zhang & Goldberg, 2011; Zhang et al., 2003). White et al. (2014) showed that EVI derived from Landsat TM data provided better SOS estimates than that of NDVI in deciduous forests, possibly because of EVI being less sensitive to high biomass than NDVI. Similarly, Wu et al. (2014) found that EVI is a stronger predictor of both SOS and EOS than NDVI at four boreal deciduous forest sites. However, for needleleaf or conifer forests, EVI was not found to have better potential for phenological modeling than NDVI (Wu et al., 2014). Our results using data from 14 flux tower sites showed that neither NDVI nor EVI alone can provide consistent and robust estimates of SOS or EOS, which is consistent with previous findings (such as Hmimina et al., 2013; Shen et al., 2014).

Our newly derived phenology model based on the product of VI × CV_LST showed better performance in estimating SOS and EOS compared to NDVI or EVI. Previous analysis of White et al. (2014) suggests that EVI may have better potential than NDVI for phenological modeling for deciduous forests, and the main underlying reason being that EVI is its less sensitivity to high biomass. However, our results for the needleleaf forest sites showed that there is no evidence of better performance of EVI over NDVI for needleleaf forests as both showed statistically significant relationship for comparable number of sites for SOS and EOS. More interestingly, NDVI had significantly better performance for both SOS and EOS modeling compared with that of EVI (Fig. 9). We argue that for estimating SOS and EOS for needleleaf forest, the saturation of NDVI may not be a serious problem since green biomass will not attain its maximum value in early spring and autumn, which are critical periods for estimating SOS and EOS from remote sensing signals.

4.3. Directly relating phenology with VI and LST

We directly related GPP-derived phenology (i.e., SOS and EOS) to the product of VI and LST variables. A potential uncertainty of this algorithm is the time lag effect of plant productivity to temperature. For example, one single cold day may prevent the leaf out in the next a few days. Previous analyses showed that the time lag at the monthly scale of the vegetation responses to climate to generally be shorter than 0.25 (Anderson et al., 2010; Chen et al., 2014). In our analysis, we suggest that it is reasonable to directly relate phenological transitions derived from GPP to the product of VI and LST. First, we showed the monthly temporal patterns of GPP, NDVI/EVI and temperature for all flux sites (see Fig. 4) and we found that for these evergreen needleleaf forest ecosystems, there is no apparent time lag between productivity and temperature at monthly temporal scale. Second, a recent study of Wu et al. (2015) demonstrated that at the middle and high latitudes (30N–90N, 30S–90S), vegetation productivity has the greatest correlation with temperature in the same month and does not exhibit evident lag effects. In particular, even at low latitudes, more than 70% of evergreen forests do not have time lag effects between productivity and temperature (Wu et al., 2015). Therefore, the variation of temperature is reflected in both GPP (i.e., GPP derived SOS and EOS) and remote sensing vegetation measures so that our algorithm could be useful for most evergreen needleleaf forests over this region.

4.4. Comparison between SOS and EOS

It has been recognized that for most terrestrial ecosystems, the SOS is more likely to be modeled at higher accuracy than EOS from remote sensing observations (Guyon et al., 2011; Hufkens et al., 2012; Melaas, Friedl, et al., 2013; Shen et al., 2014), and this is also confirmed in our analysis. It because plants experience a much longer and slow change of canopy greenness and thus photosynthesis during senescence as compared to onset of canopy greenness in spring (Richardson et al.,

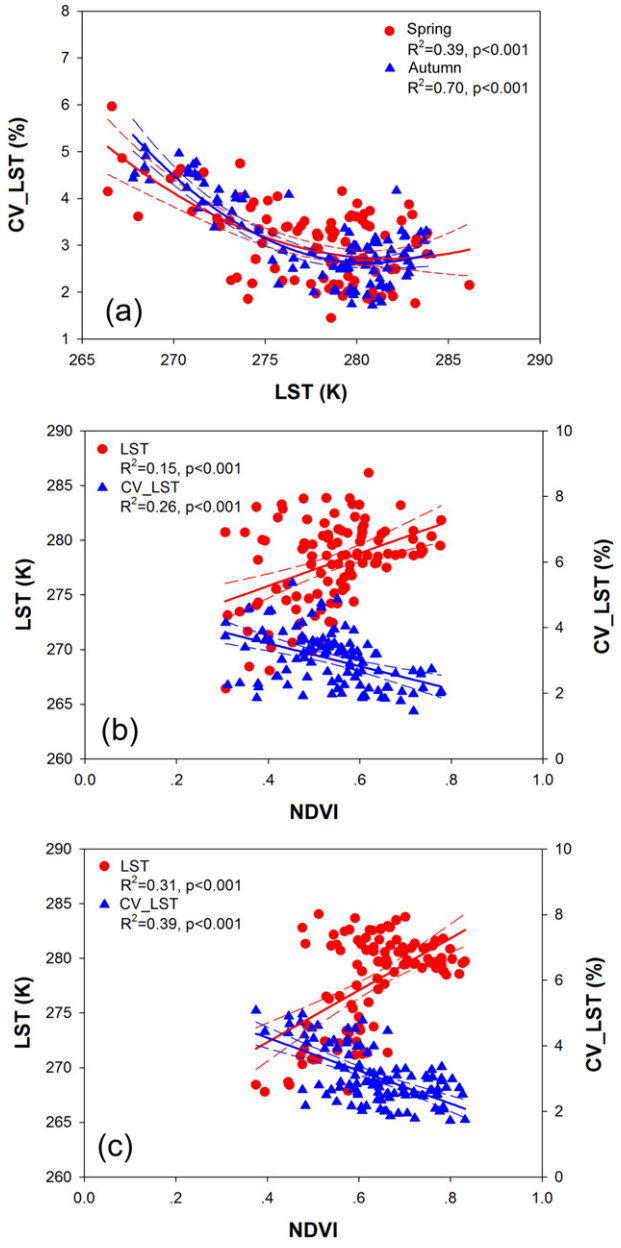

Fig. 10. Relationship between (a) the MODIS Land surface temperature (LST) and its coefficients of variation (CV_LST) in spring and autumn, and between NDVI and LST/LST_CV in (b) spring and (c) autumn for all sites.

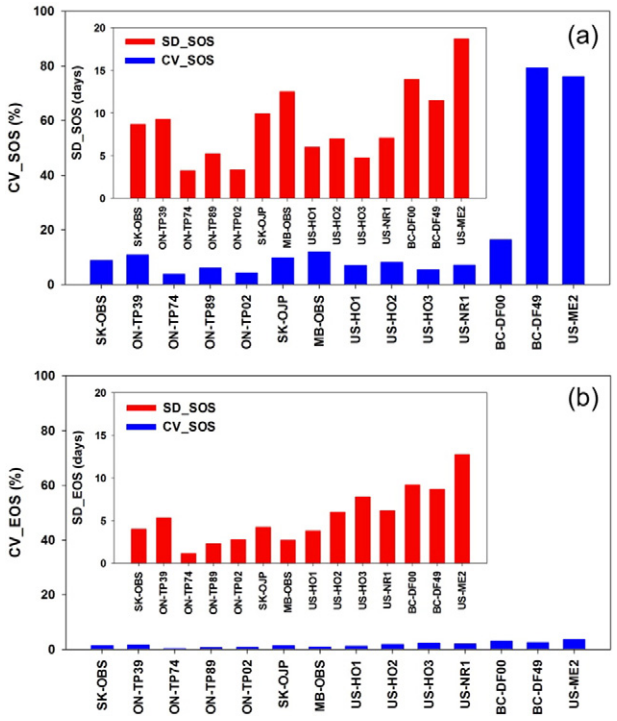

Fig. 11. Comparison between flux measured (a) standard deviation (SD_SOS) and coefficients of variation of start of growing season (CV_SOS) in spring an (b) standard deviation (SD_EOS) and coefficients of variation of end of growing season (CV_EOS) in autumn for all sites in this study.

2013). Using flux tower measured GPP records, we found that for each site, SD_SOS was significantly larger than SD_EOS using the two tail t-test ($p = 0.038$) (Fig. 11). Coefficient of variation of SOS (CV_SOS) was also significantly higher than CV_EOS ($p = 0.030$). For the overall dataset, mean value of SD_SOS and CV_SOS were 8.7 days and 18.2%, respectively, both longer than that of SD_EOS (5.5 days) and CV_EOS (1.7%).

4.5. Study limitations

We proposed a new model using MODIS-based VIs and LST to estimate SOS and EOS of 14 North American needleleaf forest flux tower sites. Additional validation was conducted using canopy-based camera data at 5 sites. The results were promising with significant improvements in modeled SOS and EOS as compared to previous methods based on single VIs. Even though, there are several issues that might be considered in its further applications. The new model, i.e., NDVI/EVI × CV_LST might be more appropriate in phenology studies in boreal and temperate forests because temperature is a main determinant of plant growth in these regions. Second, complicated interaction between multiple climate variables and plant phenology makes it challenging to derive a universal model that is able to depict interannual variability of phenology for mountainous ecosystems, especially for US-NR1 in this study (Monson et al., 2005; Wu, Chen, Black, et al., 2013). This issue requires further investigation between plant phenology and other environmental factors (e.g., soil temperature and water status) if the new phenology model is to be included in ecosystem models. While the GPP threshold method has been well demonstrated to be useful in determining land surface phenology of forests (Garrity et al., 2011; Richardson et al., 2010; Wu et al., 2014), confidence in this new model will be enhanced if more data from various plant functional types are included. The final aspect is the footprint of the MODIS observations that we directly used the MODIS Surface Reflectance product. However, the footprint sizes and locations of observations used to grid for the MODIS grid cell vary with viewing geometries and they may be not necessarily always have common area or overlap each other (Zhang, Cheng, Lyapustin, Wang, Gao, et al., 2014; Zhang, Cheng, Lyapustin, Wang, Xiao, et al., 2014). Therefore, a potential way to improve the accuracy of modeled phenology may lie in the way that we consider the grid location and grid size of MODIS observations.

5. Conclusions

Using continuous multiple-year flux measurements at 14 flux tower sites for needleleaf forest in North America, we evaluated the potential of MODIS land surface reflectance and temperature data for estimating the start and the end of the growing season. We found that a single VI, neither NDVI nor EVI, was not able to accurately predict SOS and EOS because of the low intra-annual variations of canopy greenness for the needleleaf or conifer forests. The MODIS LST might be a good proxy

for SOS modeling but not for EOS. A particularly important finding of our results was that the land surface temperature variability is more useful than average temperature itself in indicating plant phenology, which might be overlooked in precious studies in literature. Based on these findings, we proposed a new model that incorporated both a VI and CV_LST, which showed improved estimates of both SOS and EOS with RMSE within 11.7 days and 5.6 days, respectively. Additional validation at five PhenoCam sites also demonstrated the usefulness of the model. Further analysis might be necessary to extend our results for other biomes or plant functional types (e.g., grasslands and shrub lands) and for other regions (e.g., Mediterranean, arid ecosystems) which have more complex interactions between climate and plant phenology.

Acknowledgments

This work used data from flux sites from both the AmeriFlux and Fluxnet-Canada and we appreciate the flux PIs providing these valuable data and helpful explanations. Data collection and analyzing from PhenoCam sites are also appreciated. This work was funded by the National Natural Science Foundation of China (41371013, 41522109), the Open Research Fund of State Key Laboratory of Remote Sensing Science (OFSLRSS201413), the International Postdoctoral Funding to A. Gonsamo (Grant No. 2015PE030), and the Dean funding to C. Wu.

References

Anderson, L. O., Malhi, Y., Aragão, L. E., Ladle, R., Arai, E., Barbier, N., & Phillips, O. (2010). Remote sensing detection of droughts in Amazonian forest canopies. *New Phytologist*, *187*(3), 733–750.

Arain, M. A., Yaun, F., & Black, T. A. (2006). Soil–plant nitrogen cycling modulated carbon exchanges in a western temperate conifer forest in Canada. *Agricultural and Forest Meteorology*, *140*, 171–192.

Baldocchi, D. D., Falge, E., Gu, L. H., Olson, R., Hollinger, D., Running, S., et al. (2001). FLUXNET: A new tool to study the temporal and spatial variability of ecosystem-scale carbon dioxide, water vapor, and energy flux densities. *Bulletin of the American Meteorological Society*, *82*, 2415–2434.

Barr, A., Black, T. A., & McCaughey, H. (2009). Climatic and phenological controls of the carbon and energy balances of three contrasting boreal forest ecosystems in western Canada. In A. Noormets (Ed.), *Phenology of ecosystem processes* (pp. 3–34). New York, NY: Springer.

Barr, A. G., Black, T. A., Hogg, E. H., Kljun, N., Morgenstern, K., & Nesic, Z. (2004). Interannual variability in the leaf area index of a boreal aspen-hazelnut forest in relation to net ecosystem production. *Agricultural and Forest Meteorology*, *126*(3–4), 237–255.

Barr, A. G., Richardson, A. D., Hollinger, D. Y., Papale, D., Arain, M. A., Black, T. A., ... Schaeffer, K. (2013). Use of change-point detection for friction–velocity threshold evaluation in eddy-covariance studies. *Agricultural and Forest Meteorology*, *171-172*, 31–45.

Bergeron, O., Margolis, H. A., Coursolle, C., & Giasson, M. (2008). How does forest harvest influence carbon dioxide fluxes of black spruce ecosystems in eastern North America? *Agricultural and Forest Meteorology*, *148*, 537–548.

Black, T. A., Chen, W. J., Barr, A. G., Arain, M. A., Chen, Z., Nesic, Z., ... Yang, P. C. (2000). Increased carbon sequestration by a boreal deciduous forest in years with a warm spring. *Geophysical Research Letters*, *27*, 1271–1274.

Chen, B., Coops, N. C., Fu, D., Margolis, H. A., Amiro, B. D., Barr, A. G., ... Wofsy, S. C. (2011). Assessing eddy-covariance flux tower location bias across the Fluxnet-Canada Research Network based on remote sensing and footprint modelling. *Agricultural and Forest Meteorology*, *151*, 87–100.

Chen, J. M., Ju, W., Cihlar, J., Price, D., Liu, J., Chen, W., ... Barr, A. (2003). Spatial distribution of carbon sources and sinks in Canada's forests based on remote sensing. *Tellus B*, *55*, 622–642.

Chen, T., De Jeu, R., Liu, Y. Y., Van der Werf, G. R., & Dolman, A. J. (2014). Using satellite based soil moisture to quantify the water driven variability in NDVI: A case study over mainland Australia. *Remote Sensing of Environment*, *140*, 330–338.

Desai, A. R., Richardson, A. D., Moffat, A. M., Kattge, J., Hollinger, D. Y., Barr, A., et al. (2008). Cross site evaluation of eddy covariance GPP and RE decomposition techniques. *Agricultural and Forest Meteorology*, *148*, 821–838.

Dunn, A. L., Barford, C. C., Wofsy, S. C., Goulden, M. L., & Daube, B. C. (2007). A long-term record of carbon exchange in a boreal black spruce forest: Means, responses to interannual variability and decadal trends. *Global Change Biology*, *13*, 577–590.

Friedl, M. A., Sulla-Menashe, D., Tan, B., Schneider, A., Ramankutty, A., Sibley, A., & Huang, X. (2010). MODIS Collection 5 global land cover: algorithm refinementsand characterization of new datasets. *Remote Sensing of Environment*, *114*, 168–182.

Fu, Y., Campioli, M., Vitasse, Y., et al. (2014). Variation in leaf flushing date influences autumnal senescence and next year's flushing date in two temperate tree species. *PNAS*, *111*, 7355–7360.

Ganguly, S., Friedl, M. A., Tan, B., Zhang, X., & Verma, M. (2010). Land surface phenology from MODIS: Characterization of the Collection 5 global land cover dynamics product. *Remote Sensing of Environment*, *114*, 1805–1816.

Garrity, S. R., Maurer, K. D., Mueller, K. L., Vogel, C. S., & Curtis, P. S. (2011). A comparison of multiple phenology data sources for estimating seasonal transitions in deciduous forest carbon exchange. *Agricultural and Forest Meteorology*, *151*, 1741–1752.

Gonsamo, A., Chen, J. M., Price, D. T., Kurz, W. A., & Wu, C. (2012b). Land surface phenology from optical satellite measurement and CO_2 eddy covariance technique. *Journal of Geophysical Research*, *117*. http://dx.doi.org/10.1029/2012JG002070.

Gonsamo, A., Chen, J. M., Wu, C., & Dragoni, D. (2012a). Predicting deciduous forest carbon uptake phenology by upscaling FLUXNET measurements using remote sensing data. *Agricultural and Forest Meteorology*, *165*, 127–135.

Guyon, D., Guillot, M., Vitasse, Y., Cardot, H., Hagolle, O., Delzon, S., et al. (2011). Monitoring elevation variations in leaf phenology of deciduous broadleafforests from SPOT/VEGETATION time-series. *Remote Sensing of Environment*, *115*, 615–627.

Hmimina, G., Dufrêne, E., Pontailler, J. Y., Delpierre, N., Aubinet, M., Caquet, B., et al. (2013). Evaluation of the potential of MODIS satellite data to predict vegetation phenology in different biomes: An investigation using ground-based NDVI measurements. *Remote Sensing of Environment*, *132*, 145–158.

Hollinger, D. Y., Aber, J., Dail, B., Davidson, E. A., Goltz, S. M., Hughes, H., et al. (2004). Spatial and temporal variability in forest-atmosphere CO_2 exchange. *Global Change Biology*, *10*, 1689–1706.

Huete, A., Didan, K., Miura, T., Rodriguez, E. P., Gao, X., & Ferreira, L. G. (2002). Overview of the radiometric and biophysical performance of the MODIS vegetation indices. *Remote Sensing of Environment*, *83*, 195–213.

Hufkens, K., Friedl, M., Sonnentag, O., Braswell, B. H., Milliman, T., & Richardson, A. D. (2012). Linking near-surface and satellite remote sensingmeasurements of deciduous broadleaf forest phenology. *Remote Sensing of Environment*, *117*, 307–321.

IBM Corp. Released (2010). *IBM SPSS statistics for windows, version 19.0*. Armonk, NY: IBM Corp.

Jassal, R. S., Black, T. A., Spittlehouse, D. L., Brümmer, C., & Nesic, Z. (2009). Evapotranspiration and water use efficiency in different-aged Pacific Northwest Douglas-fir stands. *Agricultural and Forest Meteorology*, *149*, 1168–1178.

Jeganathan, C., Dash, J., & Atkinson, P. M. (2014). Remotely sensed trends in the phenology of northern high latitude terrestrial vegetation, controlling for land cover change and vegetation type. *Remote Sensing of Environment*, *143*, 154–170.

Jin, H., & Eklundh, L. (2014). A physically based vegetation index for improved monitoring of plant phenology. *Remote Sensing of Environment*, *152*, 512–525.

Jin, C., Xiao, X., Merbold, L., Arneth, A., Veenendaal, E., & Kutsch, W. L. (2013). Phenology and gross primary production of two dominant savanna woodland ecosystems in Southern Africa. *Remote Sensing of Environment*, *135*, 189–201.

Klosterman, S. T., Hufkens, K., Gray, J. M., Melaas, E., Sonnentag, O., Lavine, I., ... Richardson, A. D. (2014). Evaluating remote sensing of deciduous forest phenology at multiple spatial scales using PhenoCam imagery. *Biogeosciences*, *11*, 4305–4320.

Luo, X., Chen, X., Wang, L., Xu, L., & Tian, Y. (2014). Modeling and predicting spring land surface phenology of the deciduous broadleaf forest in northern China. *Agricultural and Forest Meteorology*, *198*, 33–41.

McCaughey, J. H., Pejam, M. R., Arain, M. A., & Cameron, D. A. (2006). Carbon dioxide and energy fluxes from a boreal mixedwood forest ecosystem in Ontario, Canada. *Agricultural and Forest Meteorology*, *140*, 79–96.

Melaas, E. K., Friedl, M. A., & Zhu, Z. (2013b). Detecting interannual variation in deciduous broadleaf forest phenology using Landsat TM/ETM+ data. *Remote Sensing of Environment*, *132*, 176–185.

Melaas, E. K., Richardson, A. D., Friedl, M. A., Dragoni, D., Gough, C. M., Herbst, M., ... Moors, E. (2013a). Using FLUXNET data to improve models of springtime vegetation activity onset in forest ecosystems. *Agricultural and Forest Meteorology*, *171*, 46–56.

Monson, R. K., Sparks, J. P., Rosenstiel, T. N., Scott-Denton, L. E., Huxman, T. E., Harley, P. C., et al. (2005). Climatic influences on net ecosystem CO_2 exchange during the transition from wintertime carbon source to springtime carbon sink in a high-elevation, subalpine forest. *Oecologia*, *146*, 130–147.

Pan, Y., Birdsey, R. A., Fang, J., Houghton, R., Kauppi, P. E., Kurz, W. A., et al. (2011). A large and persistent carbon sink in the world's forests. *Science*, *333*(6045), 988–993.

Papale, D., & Valentini, A. (2003). A new assessment of European forests carbon exchange by eddy fluxes and artificial neural network spatialization. *Global Change Biology*, *9*, 525–535.

Piao, S., Fang, J., Zhou, L., et al. (2006). Variations in satellite-derived phenology in China's temperate vegetation. *Global Change Biology*, *12*, 672–685.

Reichstein, M., Falge, E., Baldocchi, D., Papale, D., Aubinet, M., Berbigier, P., Bernhofer, C., et al. (2005). On the separation of net ecosystem exchange into assimilation and ecosystem respiration: review and improved algorithm. *Global Change Biology*, *11*, 1424–1439.

Reyer, C. P. O., Leuzinger, S., Rammig, A., Wolf, A., Bartholomeus, R. P., Bonfante, A., ... Pereira, M. (2013). A plant's perspective of extremes: Terrestrial plant responses to changing climatic variability. *Global Change Biology*, *19*, 75–89.

Richardson, A. D., Black, T. A., Ciais, P., Delbart, N., Friedl, M. A., Gobron, N., et al. (2010). Influence of spring and autumn phenological transitions on forest ecosystem productivity. *Philosophical Transactions of the Royal Society B: Biological Sciences*, *365*, 3227–3246.

Richardson, A. D., Keenan, T. F., Migliavacca, M., Ryu, Y., Sonnentag, O., & Toomey, M. (2013). Climate change, phenology, and phenological control of vegetation feedbacks to the climate system. *Agricultural and Forest Meteorology*, *169*, 156–173.

Ryu, Y., Lee, G., Jeon, S., Song, Y., & Kimm, H. (2014). Monitoring multi-layer canopy spring phenology of temperate deciduous and evergreen forests using low-cost spectral sensors. *Remote Sensing of Environment*, *149*, 227–238.

Sakamoto, T., Gitelson, A. A., & Arkebauer, T. J. (2013). MODIS-based corn grain yield estimation model incorporating crop phenology information. *Remote Sensing of Environment*, *131*, 215–231.

Sakamoto, T., Wardlow, B. D., Gitelson, A. A., Verma, S. B., Suyker, A. E., & Arkebauer, T. J. (2010). A two-step filtering approach for detecting maize and soybean phenology with time-series MODIS data. *Remote Sensing of Environment*, *114*, 2146–2159.

Shen, M., Tang, Y., Desai, A. R., et al. (2014). Can EVI-derived land surface phenology be used as a surrogate for phenology of canopy photosynthesis? *International Journal of Remote Sensing*, *35*, 1162–1174.

Sims, D. A., Rahman, A. F., Cordova, V. D., El-Masri, B. Z., Baldocchi, D. D., Bolstad, P. V., ... Xu, L. (2008). A new model of gross primary productivity for North American ecosystems based solely on the enhanced vegetation index and land surface temperature from MODIS. *Remote Sensing of Environment*, *112*, 1633–1646.

Sonnentag, O., Hufkens, K., Teshera-Sterne, C., Young, A. M., Friedl, M., Braswell, B. H., et al. (2012). Digital repeat photography for phenological research in forest ecosystems. *Agricultural and Forest Meteorology*, *152*, 159–177.

Suni, T., Berninger, F., Vesala, T., et al. (2003). Air temperature triggers the recovery of evergreen boreal forest photosynthesis in spring. *Global Change Biology*, *9*, 1410–1425.

Thomas, C. K., Law, B. E., Irvine, J., Martin, J. G., Pettijohn, J. C., & Davis, K. J. (2009). Seasonal hydrology explains interannual and seasonal variation in carbon and water exchange in a semiarid mature ponderosa pine forest in central Oregon. *Journal of Geophysical Research*, *114*, G04006. http://dx.doi.org/10.1029/2009JG001010.

Tucker, C. J., & Sellers, P. J. (1986). Satellite remote sensing of primary production. *International Journal of Remote Sensing*, *7*, 1395–1416.

Wan, Z. (2008). New refinements and validation of the MODIS Land-Surface Temperature/Emissivity products. *Remote Sensing of Environment*, *112*, 59–74.

Wharton, S., Falk, M., Bible, K., Schroeder, M., & Paw, U. K. T. (2012). Old-growth CO_2 flux measurements reveal high sensitivity to climate anomalies across seasonal, annual and decadal time scales. *Agricultural and Forest Meteorology*, *161*, 1–14.

Wheeler, T. R., Craufurd, P. Q., Ellis, R. H., Porter, J. R., & Prasad, P. V. (2000). Temperature variability and the yield of annual crops. *Agriculture, Ecosystems & Environment*, *82*, 159–167.

White, M. A., de Beurs, K. M., Didan, K., Inouye, D. W., Richardson, A. D., Jensen, O. P., et al. (2009). Intercomparison, interpretation, and assessment of spring phenology in North America estimated from remote sensing for 1982–2006. *Global Change Biology*, *15*, 2335–2359.

White, K., Pontius, J., & Schaberg, P. (2014). Remote sensing of spring phenology in northeastern forests: A comparison of methods, field metrics and sources of uncertainty. *Remote Sensing of Environment*, *148*, 97–107.

Wu, C., Chen, J. M., Black, T. A., Price, D. T., Kurz, W. A., Desai, A. R., et al. (2013a). Interannual variability of net ecosystem productivity in forests is explained by carbon flux phenology in autumn. *Global Ecology and Biogeography*, *22*, 994–1006.

Wu, C., Chen, J. M., Desai, A. R., Lafleur, P. M., & Verma, S. B. (2013b). Positive impacts of precipitation intensity on monthly CO_2 fluxes in North America. *Global and Planetary Change*, *100*, 204–214.

Wu, C., Chen, J. M., Gonsamo, A., Price, D. T., Black, T. A., & Kurz, W. A. (2012). Interannual variability of carbon sequestration is determined by the lag between ends of net uptake and photosynthesis: Evidence from long records of two contrasting forest stands. *Agricultural and Forest Meteorology*, *164*, 29–38.

Wu, C., Gonsamo, A., Gough, C. M., Chen, J. M., & Xu, S. (2014). Modeling growing season phenology of North American forests using seasonal mean vegetation indices from MODIS. *Remote Sensing of Environment*, *147*, 79–88.

Wu, C., Hou, X., Peng, D., Gonsamo, A., & Xu, S. (2016). Land surface phenology of China's temperate ecosystems over 1999–2013: Spatial–temporal patterns, interaction effects, covariation with climate and implications for productivity. *Agricultural and Forest Meteorology*, *216*, 177–187.

Wu, D., Zhao, X., Liang, S., Zhou, T., Huang, K., Tang, B., & Zhao, W. (2015). Time-lag effects of global vegetation responses to climate change. *Global Change Biology*. http://dx.doi.org/10.1111/gcb.12945.

Xiao, X., Hagen, S., Zhang, Q., Keller, M., & Moore, B., III (2006). Detecting leaf phenology of seasonally moist tropical forests in South America with multi-temporal MODIS images. *Remote Sensing of Environment*, *103*, 465–473.

Zhang, X., & Goldberg, M. D. (2011). Monitoring fall foliage coloration dynamics using time-series satellite data. *Remote Sensing of Environment*, *115*, 382–391.

Zhang, Q., Cheng, Y., Lyapustin, A. L., Wang, Y., Gao, F., Suyker, A., ... Middleton, E. M. (2014a). Estimation of crop gross primary production (GPP): fAPARchl versus MOD15A2 FPAR. *Remote Sensing of Environment*, *153*, 1–6.

Zhang, Q., Cheng, Y., Lyapustin, A. I., Wang, Y., Xiao, X., Suyker, A., ... Middleton, E. M. (2014b). Estimation of crop gross primary production (GPP): I. Impact of MODIS observation footprint and impact of vegetation BRDF characteristics. *Agricultural and Forest Meteorology*, *191*, 51–63.

Zhang, X., Friedl, M. A., & Schaaf, C. B. (2006). Global vegetation phenology from Moderate Resolution Imaging Spectroradiometer (MODIS): Evaluation of global patterns and comparison with in situ measurements. *Journal of Geophysical Research – Biogeosciences*, *111*. http://dx.doi.org/10.1029/2006JG000217.

Zhang, X., Friedl, M. A., Schaaf, C. B., Strahler, A. H., Hodges, J. C. F., Gao, F., et al. (2003). Monitoring vegetation phenology using MODIS. *Remote Sensing of Environment*, *84*, 471–475.